https://doi.org/10.5194/egusphere-2025-1905
Preprint. Discussion started: 12 May 2025

Application of Self-Organizing Maps to characterize subglacial bedrock properties in East Antarctica based on gravity, magnetic and radar data

Jonas Liebsch[1,*], Jörg Ebbing[1], Kenichi Matsuoka[2]

[1]Institue of Geosciences, Kiel University, Germany
[2] Norwegian Polar Institute, Tromsø, Norway
[*]Now at: University of Iceland, Reykjavik, Iceland

Correspondence to: Jörg Ebbing (joerg.ebbing@ifg.uni-kiel.de)

Abstract. Subglacial bedrock properties are a key to understand and predict the dynamics and future evolution of the Antarctic Ice Sheet. However, the ice sheet bed is largely inaccessible for direct sampling. Therefore, it is crucial to efficiently combine various attributes derived from satellite and airborne geophysical surveys to characterize subglacial properties. To reduce subjective choices in the joint analysis of data and related biases, we evaluate a Self-Organizing Map (SOM), an unsupervised machine learning technique. The concept of SOMs, an unsupervised machine learning approach, is briefly discussed, but we focus on data selection and their associated attributes for the case at hand. For this, we analysis the correlation between attributes in order to provide a validation of an appropriate choice. The SOM is trained on attributes derived from gravity, magnetics and ice-penetrating radar data for the Wilkes Land area in East Antarctica, a region where basal conditions may be of high importance to ice sheet flow and corresponding sea level rise, and where also suitable data sets for the application of the SOM exist. In contrast to the earlier studies, our approach uses original line data as far as possible, which have much higher resolution/sampling than in smooth gridded products, which were used for previous analyses. Previous analysis indicated the presence of both crystalline basement and sedimentary basins in the area, and our SOM shows a remarkable agreement, but suggests some points of difference, as for example, some highlands appear similar on previous interpretations, but have quite dissimilar physical settings, which is also expressed in our results. These variations can potentially be exploited further in describing subglacial properties and the coupling between bed and overlying ice-sheets.

https://doi.org/10.5194/egusphere-2025-1905
Preprint. Discussion started: 12 May 2025

1 Introduction

Subglacial bedrock properties, are one of the key components in an improved understanding of the Antarctic Ice Sheet (e.g. Aitken et al. 2023, Bell et al. 2008, McCormack et al. 2022). Especially, the properties at the ice sheet bed (ice-rock interface) can have a significant impact on ice flow dynamics as roughness and consolidation of the bed, as well as hydro(geo)logical processes, impact friction and basal sliding processes, and therefore, ice flow velocities (Koellner et al., 2019). Hereby, especially the presence of layers of sediments and sedimentary rocks at the base of the ice are of interest as these can affect basal friction, water flow and advect geothermal heat (e.g. Koellner, et al. 2019, Zoet and Iverson, 2020, Li et al. 2022, Aitken et al. 2023).

There are very few seismic lines on the Antarctic continent suitable for resolving the upper crust (e.g. Anandakrishnan et al. 1998, Bayer et al. 2009, Leitchenkov et al. 2016), so geological models are conventionally based on interpretation of bed topography (.g. Taylor 1914, Elliot, 1975, Jordan et al. 2020), airborne magnetic or gravity datasets (e.g. Ferraccioli et al. 2002, 2009, McLean et al. 2009, Aitken et al. 2014, Kim et al. 2022), or a combination of those (e.g. Li et al., 2023, Wu et al. 2023). Especially, aeromagnetic data is the best suited geophysical data set to map subglacial geology (Betts et al. 2024). However, the interpretation requires some form of constraint to overcome the inherent ambiguities. Therefore, the combination with other geophysical data sets in an integrated manner is often the most sensible choice (e.g. Jordan et al. 2023, Lowe et al. 2024a, b).

Airborne radar data are complimentary and well-suited for imaging within the ice but are almost entirely reflected at the ice-rock interface. Therefore, radar can provide characteristics of the bed-ice interface, but physical properties of the bedrock itself are difficult to derive. Still, detailed morphology and inferred attributes like roughness can indicate some near-surface geological characteristics (e.g. Shepherd et al. 2006, Rippin et al., 2014; Jordan et al., 2010, Jordan et al. 2023), as an area with increased roughness can be inferred to have a more erosion-resistant bed. However, the flow speed of the ice sheets from current and past events also impacts erosion and modifies the roughness (Jamieson et al., 2014). Hence, combination of these data sets might provide a mean to overcome some of the limitations.

Recently, Aitken et al. (2023) presented a detailed classification of geological bed type in Antarctica by analysing multiple geophysical data sets and models. Hereby, they compiled and synthesized available data and models into a classification map. While Aiken et al. (2023) presented continent-wide, detail classification of geological bed types, it is in part subject to interpretations and remains equivocal at some locations due to complex geology and/or limited data coverages. Another limitation are the different methods used in establishing the subglacial property models subsequently compiled. Please see Aitken et al. (2023) for more details on this.

Machine learning and statistical based methods are nowadays popular approaches for less heterogenous models. Such methods were applied to estimate geothermal heat flow (Lösing and Ebbing, 2021, Stål et al. 2021) and presence of sedimentary rocks (Li et al., 2022). Especially, machine learning methods such as gradient boosting regression tree have become popular to map subglacial properties in both Greenland and Antarctica (e.g. Rezvanbehbahani et al. 2019, Lösing & Ebbing, 2021, Li et al. 2022, Colgan et al. 2023). These studies are commonly on the scale of an entire continent as these approaches rely on training

https://doi.org/10.5194/egusphere-2025-1905
Preprint. Discussion started: 12 May 2025

datasets of reasonable size, which is often a limiting factor as data coverage and quality is variable, and the subjective choice of which data type to consider as suitable.

As an alternative, we employ here Self-Organizing Maps (SOMs; Kohonen, 1990) to exploit local information. SOMs are an unsupervised machine learning approach, where similarities within different data types are estimated without assigning these to predefined categories. In the following, we will shortly summarize the concept of SOMs and introduce the data and attribute used for our analysis. We discuss our results both in comparison to the classification by Aitken et al. (2023), and with respect to the choice of input data by studying correlation between them.

The study area is in Wilkes Land, East Antarctica (Figure 1), chosen for the excellent coverage with line data and as it is a key region for studying the role of tectonic boundary conditions on the behaviour of the East Antarctic Ice Sheet (Aitken et al. 2014, McCormack et al. 2022).

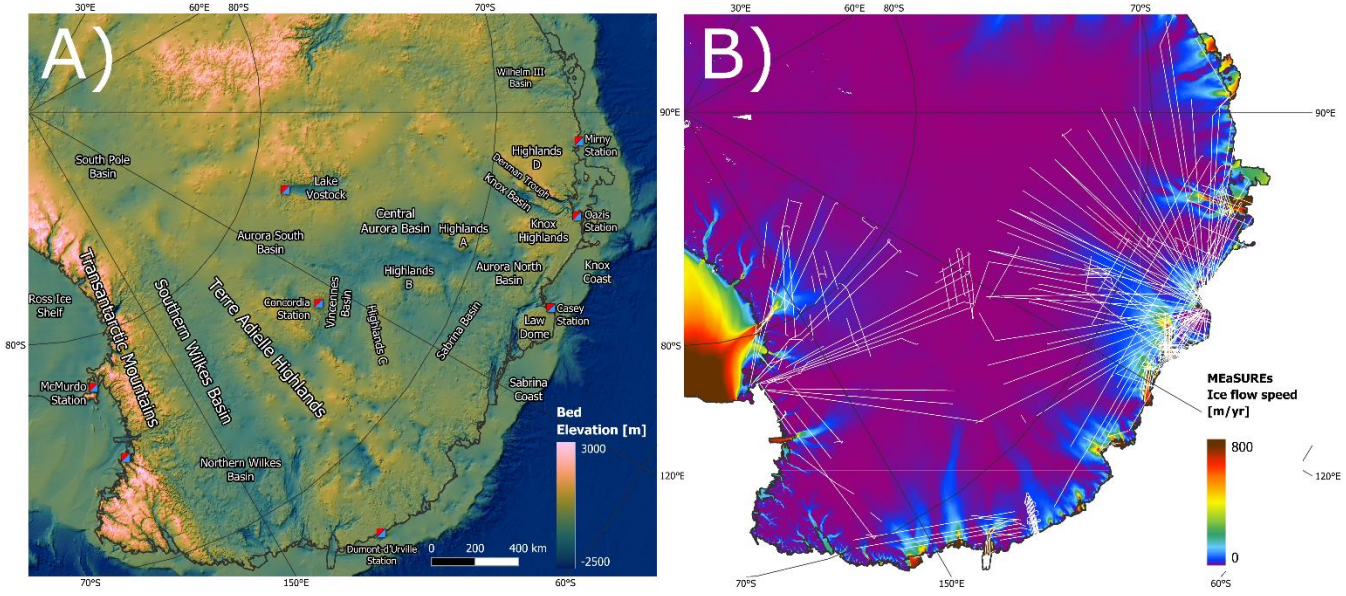

Figure 1: Wilkes Land, East Antarctica: A) Bed elevation from Bedmachine (Morlighem, 2020, 2022). Important subglacial and geographical features are annotated. B) Ice flow speed (Mouginot, 2017), overlain by NASA Operation Ice Bridge (OIB) flightlines used in this study.

2 Self-Organizing Maps

SOMs, unlike other unsupervised learning algorithms, do not attempt to categorize data; rather, they reduce the dimensionality of a complex dataset. In our example, we will map the three datasets (bed elevation, gravity, and magnetics) and the related attributes into a 2D space (map) representation. In this space, similar data points are placed in proximity to each other, enabling the identification of clusters. In the following, we briefly explain the concept of SOMs, but the interested reader is referred to e.g. Klose (2006) for a more detailed description.

https://doi.org/10.5194/egusphere-2025-1905
Preprint. Discussion started: 12 May 2025

Self-Organizing Maps (SOMs) are a simple neural network consisting of a single layer. Each neuron represents a cell on the two-dimensional map with one weight for every dimension of the input data. Neuron j is described by its weights m_j. The weights of a cell translate to a value for each data type (e.g. bed roughness, magnetic anomaly, …), they can therefore also be understood as coordinate in the multidimensional data space.

For a given data point x_i, a best-matching neuron with the weights m_b is chosen in such a way that the Euclidean distance between x_i and m_b is minimized:

$$\|\boldsymbol{x_i} - \boldsymbol{m_b}\| = \min_j\{\|\boldsymbol{x_i} - \boldsymbol{m_j}\|\} \quad (1)$$

The weights of m_b and the point x_i are therefore very similar. Besides the weights, a neuron also has a location on the self-organizing map, which describes the coordinate r in a two-dimensional space.

The network is trained iteratively t times for a random-chosen input data point x_i. The best-matching neuron for this data point is determined, and then the weights of it and its neighbours are adjusted towards x_i. The value of the adjustment is determined by a neighbourhood function $h_{bj}(t)$, it will be 1 for the best-matching neuron and decay as further the neuron is away from the best matching neuron on the two-dimensional map. As a result of this neighbourhood function, the map is trained in a way that ensures neighbouring cells on the map have similar weights and therefore will have similar data points mapping to the same cluster. In addition, for convergence purposes a time-dependent learning rate $\alpha(t)$ is employed.

The training of a cell $m_j(t)$ can be expressed as follows:

$$m_j(t+1) = m_j(t) + \alpha(t)h_{bj}(t)\left[x_i - m_j(t)\right] \quad (2)$$

The choice of the neighbourhood function can vary, and we utilise a Gaussian function:

$$h_{bj}(t) = \exp\left(-\frac{||r_b - r_j||}{2\sigma^2(t)}\right) \quad (3)$$

Here, r_b and r_j represent the locations of the best-matching neuron and the neuron to be trained on the self-organizing map, respectively. The parameter σ influences the smoothness of the computed map.

It is important to keep in mind that the two-dimensional SOM does not represent a geographic map, it is an arbitrary lower dimensional representation of the higher dimensional training dataset. E.g. an area with crystalline rocks with high gravity, and magnetic value, as well as a rough bed, will appear close to similar areas, even though they are geographically far apart.

3 Study area, Data, and SOM analysis

3.1 Study area

As mentioned before the study area in Wilkes Land, East Antarctica (Figure 1), has been chosen due to its excellent data coverage and its importance for our understanding of evolution of the East Antarctic Ice Sheet. The area has recently gained attention due to its increasing loss in ice mass (e.g. Davison et al. 2023) and rapid basal melt rates its surrounding ice shelves (Rignot et al., 2013) and consequently its massive potential for sea-level rise. The Wilkes Land ice catchments may be more

https://doi.org/10.5194/egusphere-2025-1905
Preprint. Discussion started: 12 May 2025

vulnerable to change than other catchments in the East Antarctic Ice Sheet, as the ice sheet bed is predominantly below sea level (Fretwell et al., 2013) and is subject to marine ice sheet instability.

As explained by Aitken et al. (2014), the differences in the bed conditions related to topography and geology, provide persistent and strong boundary conditions on the East Antarctic Ice Sheet (see also McCormack et al. 2022), and a geological record of a substantial past history of collapse and readvance exists (Aiken et al. 2016). Aitken et al. (2014) provided a detailed interpretation of subglacial geology using gravity, magnetic and subglacial topography data and studying the links to Southern Australia, as the conjugate neighbour during Gondwana, but details remain to be analysed as also seen on the recent classification of geological bed type by Aitken et al. (2023). Here, we explore the possibility to provide an additional level of details using SOMs, making as well use of the availability of high-quality airborne data sets.

3.2 Datasets

We use the NASA Operation Ice Bridge (OIB) dataset collected between 2009 and 2012 (Figure 2) and high-level data products derived from this dataset. The Radar Data were recorded using the Hi-Capability Radar Sounder (HiCARS) Version 1 and later on Version 2 instrument. (MacGregor et al. 2021, https://nsidc.org/data/icebridge). We used the derived bed elevation from the radargrams (Blankenship et al. 2012, 2017). This dataset, however, includes a number of short-distance data gaps even in areas where bed echo is clearly visible in the radargram. This leads to larger gaps in derived attributes, as can be seen in Eisen et al. (2020). We applied an optimisation algorithm which filled each gap with sufficiently strong returns automatically. It specifically maximised the amplitude and the vertical gradient of the amplitude along the chosen bed elevation while minimizing the length of the bed elevation path (Liebsch 2023).

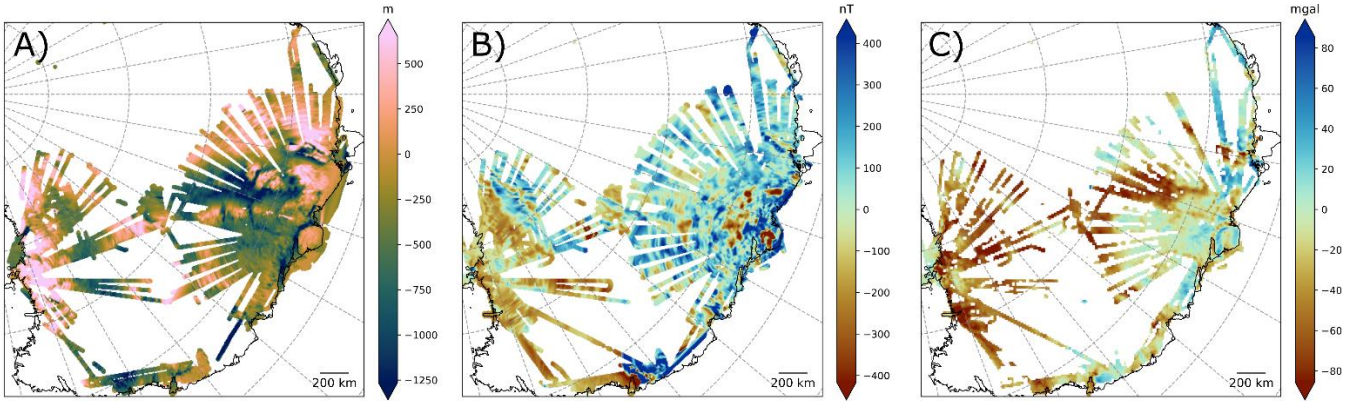

Figure 2: Data sources for the SOM: A) Bed elevation from radar data (NASA Operation Ice Bridge), B) Magnetic anomaly (taken from ADMAP-2 (Golynsky et al. 2018), C) Bouguer gravity anomaly (after Scheinert et al. 2016).

Magnetic data are taken from the ADMAP-2 compilation (Golynsky et al., 2018) along the OIB flight lines. In the supplementary database Golynsky et al., 2018), the processed line data from the individual surveys are available, which are the basis for the ADMAP-2 map. Compared to the original data, data are slightly smoothed, but suitable for our approach. For details on the magnetic processing, please see Golynsky et al. (2006, 2018).

https://doi.org/10.5194/egusphere-2025-1905
Preprint. Discussion started: 12 May 2025

Gravity were as well collected as part of the OIB surveys. Unfortunately, the available gravity data have data gaps and only parts of the data is available in a pre-processed format (see coverage in MacGregor et al. 2021). We initially planned to reprocess the data, but due to the absence of full information about the measurements, that become impossible to us. Instead, we use the compilation from Scheinert et al. (2016). This 10-km-grid dataset has been sampled along the flight lines to treat it as survey data. Although, resampling cannot provide the full resolution of the survey data, we deem this adequate for our purpose, as the distance (height) between the point of observation (airplane) and the ice-bed interface is typically 3-5 km in the study area, leading to only minor loss of information when using the gridded gravity signal.

3.3 Attributes

We used the above datasets to generate in total 29 attributes for the SOM analysis. Several attributes were derived from a single data (e.g., bed elevation), because not only the signal amplitude (e.g., bed elevation) but also the spectral characteristics and local variations (e.g., roughness) characterize the signal. This choice is subjective; therefore, rather than limiting the number of attributes we include various attributes even though some attributes presumably have very similar characteristics and including both may have little impact on our final result comparing to including only one of them. Table 1 shows the list of all the attributes and Figure 3 shows some attributes as examples.

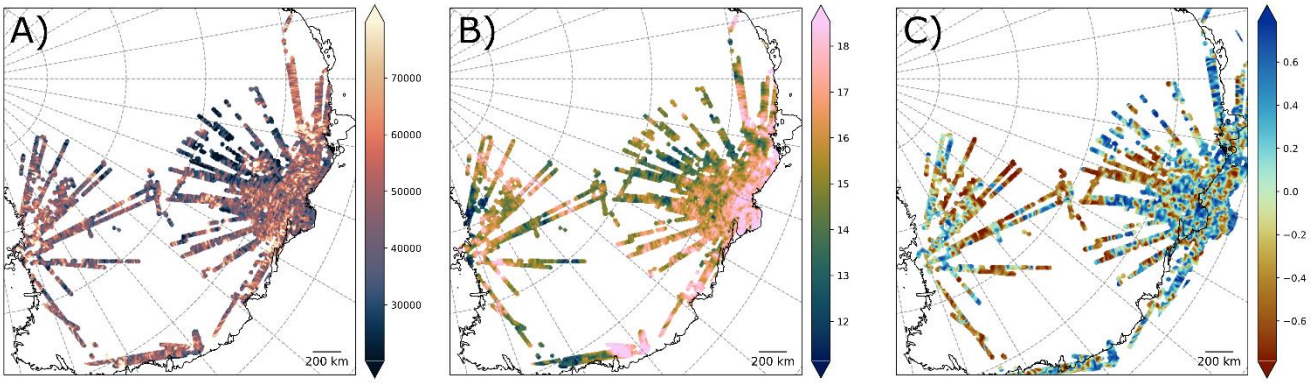

Figure 3 Example of attributes used for the SOM. A) Basal roughness ε derived from spectral domain b) Spectral Power in a 5-15 km wavelength bin from magnetic data and c) Shape index for gravity data (see text for more details).

Attributes like roughness from radar data or spectral power in the short-wavelength magnetic field provide information about the variability in subglacial properties, e.g. a crystalline basement-ice interface can be expected to have a stronger contrast and larger variability, than an incoherent bedrock (e.g. sedimentary basin) -ice interface. Other attributes based on the gravity and magnetic data (e.g. curvature) are well suited to describe the changes between data points, while features like the shape index or the tilt derivative are also known to reflect the source characteristics. For some of these, Li (2015) provides a detailed analysis of the link between source geometry and observed field.

https://doi.org/10.5194/egusphere-2025-1905
Preprint. Discussion started: 12 May 2025

	Attribute	Abbreviation
Radar /Bed Elevation (window size 10 km)	Isostatically adjusted bed elevation	Isoadjusted topo
	Spectral Centroid Bed	Centroid bed
	Roughness Attribute ξ (500 m to 2000 m wavelength)	ξ bed
	Roughness Attribute η (500 m to 2000 m wavelength)	η bed
	Variogram value (700 m to 800 m bin)	v bed
	Hurst coefficient (0 m to 1000 m)	h bed
	Moving average filtered bed elevation	Mean bed
	Standard deviation in a moving window	Stdev bed
	Kurtosis in a moving window	Kurtosis bed
	Roughnes Attribute derived from the radar Tail σ (this study)	σ
Magnetics (window size 40 km)	Magnetic Anomaly	mag
	TDX Signal	TDX mag
	Spectral Centroid	Centroid mag
	Spectral Power in the 5 to 15 km bin	Bin Power mag
	Moving average filtered magnetic anomaly	Mean mag
	Standard deviation in a moving window	Stdev mag
	Kurtosis in a moving window	Kurtosis mag
	Curvature	Curvature mag
	Vertical gradient	VG mag
	Analytical Signal	AS mag
Gravity (no Windowed Attributes)	Isostatic Anomaly	grv
	Vertical gradient	VG grv
	Analytical Signal	AS grv
	TDX Signal	TDX grv
	Mean Curvature	K_{mean} grv
	Gaussian Curvature	K_{Gauss} grv
	Min Curvature	K_{min} grv
	Max Curvature	K_{max} grv
	Shape Index	SI grv

Table 1: List of all attributes used for the SOM and explained in the text. See examples in Figure 3. See Figure 4 for the correlation between the different attributes and Figure 5 shows the weights for the attributes.

3.3.1 Radar/Bed elevation attributes

In the following, we describe the 10 attributes based on bedrock elevation and radar data. For example, roughness can be computed in various ways from the bed elevation data and used the same four roughness attributes as Eisen et al. (2020).

Isostatically adjusted bed elevation t_{iso}

Instead of using the bedrock topography, it can be useful to determine the isostatic adjusted topography t_{iso}. This attribute is the hypothetical topographic height of the landscape assuming that no ice is present. In a simplified form, disregarding dynamic effects, it can be estimated from the ice surface height s and bed elevation z using concept of isostasy after Airy with:

$$t_{iso} = (s - z) * 917/3200 + z. \quad (4)$$

Spectral Centroid Bed Centroid

The spectral centroid represents the mean of all frequencies in the spectrum f(n), weighted by their spectral power S(n).

https://doi.org/10.5194/egusphere-2025-1905
Preprint. Discussion started: 12 May 2025

$$Centroid = \frac{\sum_{n=0}^{N-1} f(n) \cdot S(n)}{\sum_{n=0}^{N-1} S(n)} \quad (5)$$

Spectral Roughness Attribute ξ

ξ is the integrated power spectral density of the bed elevation profile in a 500 m to 2000 m wavelength bin. Given with the following equation:

$$\xi = \int_{k_1}^{k_2} S(k) \mathrm{d}\, k \quad (6)$$

where S is the power spectral density and k the wavenumber in spectral domain.

Spectral Roughness Attribute η

To also capture horizontal changes in the spectral properties, Li et al. (2010) suggest to also include the integrated power spectral density of the horizontal derivative of the bed elevation ξ_{sl} analogue to ξ. The spectral roughness attribute η is defined as:

$$\eta = \frac{\xi}{\xi_{sl}} \quad (7)$$

Variogram value v

This roughness attribute is derived from a variogram derived from a window along the flight line. We use a bin covering 700 m to 800 m lag distance.

Hurst coefficient h

To complement the information on specific lag distances used in v, we also use the hurst coefficient h. The Hurst exponent corresponds to the slope of the variogram in a log-log plot and can be described as:

$$v(\Delta x) = v(\Delta x_0) \left(\frac{\Delta x}{\Delta x_0}\right)^h \quad (8)$$

Moving averaged filtered bed elevation

To avoid using the bed elevations directly and reduce noise we used a 10 km-moving average filtered bed elevation

Standard deviation in a 10 km moving window

We compute the standard deviation of the bed elevation z in a 10 km moving window.

$$\sigma_{bed} = \sqrt{\frac{1}{N} \sum_{n=1}^{N} (z_i - \overline{z})^2} \quad (9)$$

where N is the number of points in a window. And $\overline{z}$ is the mean of bed elevation in the window

Kurtosis in a 10 km moving window

Analogue to the standard deviation the kurtosis w can be computed:

https://doi.org/10.5194/egusphere-2025-1905
Preprint. Discussion started: 12 May 2025

$$w = \frac{1}{N}\sum_{n=1}^{N}\left(\frac{z_i-\bar{z}}{\sigma}\right)^4 \quad (10)$$

Bed Echo Tail Attribute σ

We additionally derive an attribute from the shape of the bed echo. Direct interpretation of reflectivity can be challenging due to unknown attenuation within the ice (Matsuoka et al. 2011). Instead, we use the tail of the bed echo, which refers to the recorded signal after the initial backscattering from the bed has occurred. The tail originates from off-nadir backscattering. A significant advantage of this approach is that a radar ray scattered at the nadir and one scattered off-nadir encounter approximately the same conditions on their way back. Consequently, the shape of the bed echo tail can be described without relying on knowledge of attenuation.

To keep the fitting procedure stable and computationally efficient across the varying conditions of the survey area we are assuming a simplistic gaussian decay of the amplitude. This is neglecting losses due to beam characteristics and spherical spreading. The amplitude A as function of incident angle φ is given as:

$$A(\varphi) = A_0 \cdot exp\left(\frac{-tan^2(\varphi)}{2\sigma^2}\right) \quad (11)$$

The bed echo tail σ can then be computed as the weighted average of $tan(\varphi)$:

$$\sigma = \frac{\sum_{i=1}^{N} A_i \cdot tan(\phi_i)}{\sum_{i=1}^{N} A_i} \quad (12)$$

3.3.2 Magnetic data attributes

For the magnetic data, 10 attributes were computed along the flight lines. Since there are few data gaps, some attributes are also computed in the spectral domain, where they are computed in a window with a length of 40 km. These attributes are standard features in describing the magnetic field. See Blakely et al. (1996) or Li et al. (2015) for more details.

Magnetic anomaly (Mag)

This corresponds to total field anomaly along the flight lines as explained above.

Tilt Derivative (TDX mag)

The TDX signal is the tilt derivative of the magnetic field (Salem et al. 2008) computed as

$$TDX = \arctan(HG/Mzz) \quad (13)$$

where HG is the total horizontal gradient and Mzz, the vertical gradient

Spectral Centroid (Centroid mag)

Typically, magnetic are inspected in a power spectrum to identify the source depth. Here, we calculate spectral centroid of the power spectrum for 40 km window using the following equation:

https://doi.org/10.5194/egusphere-2025-1905
Preprint. Discussion started: 12 May 2025

$$Centroid = \frac{\sum_{n=0}^{N-1} f(n)S(n)}{\sum_{n=0}^{N-1} S(n)} \quad (14)$$

Hereby, the spectral centroid represents the mean of all frequencies f(n) in the spectrum, weighted by their spectral power S(n).

Spectral power bin (Bin Power mag)

The spectral power of the magnetic anomaly ς_{mag}, limited to a bin of 5-15 km wavelength is calculated using the following equation:

$$\varsigma_{mag} = \int_{5\ m}^{15\ km} S_{mag}(k)dk \quad (15)$$

where S_{mag} is the classical power spectrum calculated in the wavenumber domain *k*. The range of 5-15 km has been chosen to represent subglacial sources, hereby supressing longer wavelengths due to regional sources and to suppress noise in the short-wavelength range. The intention of this attribute is to represent wavelength corresponding to the top bedrock and is shown as example in Figure 3B.

Moving average filtered magnetic anomaly (Mean mag)

This was computed by removing a linear trend of the signal in a 40 km window around each point. This attribute is enhancing the short wavelength content in the data.

Standard deviation in moving window (Stdev mag)

The attributes represent the variability of the signal in a 40 km window around each point. See attribute A8 above for details on calculation.

Kurtosis in a moving window

Kurtosis is a measure to describe the sharpness of the magnetic anomaly. See attribute A9 above for details on calculation.

Curvature (Curvature mag)

The curvature K is calculated along the flight line by

$$K = -M_{xz}/2M_z \quad (16)$$

where M_{xz} is the gradient along the flight line (x-direction) of the vertical magnetic field component M_z.

More details on curvature calculations can be found in Li et al. (2015).

Vertical gradient (VG mag)

This is the vertical derivative of the vertical magnetic field component:

$$VG = M_{zz} = \frac{\partial Mz}{\partial z} \quad (17)$$

https://doi.org/10.5194/egusphere-2025-1905
Preprint. Discussion started: 12 May 2025

Analytical signal (AS mag)

The analytical signal is calculated from the vertical gradient and the gradient along the flight line as following:

$$AS = \sqrt{M_{xz}^2 + M_{zz}^2} \quad (18)$$

Detrended Signal (Detrended mag)

The magnetic total field anomaly was detrended by removing a linear fit of the signal for 40 km window around each data point. By removing such a linear trend, the attribute is more sensitive to local scale variations.

3.3.3 Gravity data attributes

Many attributes that prove useful in identifying geological structures rely on gradients of the gravity signal. To compute these gradients, we used an equivalent source approach. The gravity grid from Scheinert et al. (2016) was inverted into a density grid of prisms extending from the ice bed to a depth of 10 km. From this density grid, all necessary gradients could be directly forward calculated following Nagy et al. (2000). The attributes are explained in the following and again, please see Blakely et al. (1996) for more details. For the curvature attributes (C5 to C9), we are following Li et al. (2015), where the full mathematical background, tests with synthetic data and an evaluation of these attributes for airborne gravity gradients can be found in. Please see also Ebbing et al. (2018) for an example for satellite gravity data for Antarctica. Please note, that all of the following attributes are calculated for grids, not along the flight lines.

Isostatic anomaly (Iso grv)

To obtain the isostatic anomaly, the free air anomaly was first mass corrected using the ice and bed elevation model Bed-Machine Antarctica v2 (Morlighem et al., 2020). To minimize isostatic effects, the undulation of the Moho boundary was estimated assuming Airy isostasy with an assumed density contrast of 530 kg/m^3 and reference depth of 25 km. The resulting undulation was then forward modelled using prisms with the same density contrast and subtracted from the mass corrected anomaly.

Vertical gradient (VG grv)

The vertical gradient of the isostatic anomaly is calculated as

$$VG = G_{zz} = \frac{\partial Iso\ grv}{\partial z} \quad (19)$$

Analytical signal (AS grv)

In contrast to the magnetic data, we calculate here the 3D analytical signal using

$$AS = \sqrt{G_{zx}^2 + G_{yz}^2 + G_{zz}^2} \quad (20)$$

where G_{xz}, G_{yz} and G_{zz} are the derivatives in the x-, y- and z-direction of the isostatic anomaly, respectively.

https://doi.org/10.5194/egusphere-2025-1905
Preprint. Discussion started: 12 May 2025

DX Signal (TDX grv)

See description for attribute B2 above.

Mean curvature (K_{mean} grv)

When curvature is used to interpret gravity anomalies, we try to delineate geometric information of subsurface structures from an observed non-geometric quantity. The mean curvature is calculated as

$$K_{mean} = \frac{G_{xx}+G_{yy}}{2G_z} \quad (21)$$

where G_{xx}, G_{yy} are the second derivatives in the x-, y-direction. G_z is the isostatic anomaly.

Gaussian Curvature (K_{Gauss} grv)

The Gaussian curvature is the product of minimum and maximum curvatures and often exhibits rapid sign changes.

$$K_{Gauss} = -\frac{G_{xx}G_{yy}-G_{xy}^2}{G_z^2} \quad (22)$$

Maximum Curvature (K_{max} grv)

From the two attributes before, we can calculate the maximum curvature:

$$K_{max} = K_{mean} + \sqrt{K_{mean}^2 - K_{Gauss}^2} \quad (23)$$

Minimum Curvature (K_{min} grv)

And similar as before, it follows the minimum curvature:

$$K_{min} = K_{mean} - \sqrt{K_{mean}^2 - K_{Gauss}^2} \quad (24)$$

Shape index (SI grv)

Maximum and minimum curvature can be combined as well to compute the shape index.

$$SI = \left(\frac{2}{\pi}\right)\arctan[(K_{max} + K_{min})/(K_{max} - K_{min})] \quad (25)$$

The shape index is shown as an example for the gravity attributes in Figure 3C.

3.4 SOM calculation, used algorithms and other considerations.

For the calculation of the SOMs, we use the existing Python package MiniSOM (Vettigli, 2018). Before training a SOM, all attributes are normalised using their standard deviation. Additionally, we removed all values deviating by more than ten standard deviations from the mean, as likely measurement errors. The threshold was arbitrarily chosen to conservatively exclude extreme outliers. All remaining points will be part of the training data set. For the interpretation, it is useful to know

https://doi.org/10.5194/egusphere-2025-1905
Preprint. Discussion started: 12 May 2025

which neurons are close to each other. Therefore, a unified distance matrix containing the distance to neighbouring neurons for each neuron is computed.

The resulting SOM has a shape of 30 by 30 and was trained using 15 000 iterations and a learning rate of 10^{-4}. σ was set to 5 to create soft weight maps and avoid overfitting. Naturally, there are numerous possibilities and parameter sets that yield acceptable results. For visual comparison only, the final map was divided in 5 clusters, where the main attributes show similar values. Boundaries were chosen in a way that neighbouring cells are distinct from each other.

4 Results and discussion

4.1 Correlation between attributes

We first examined correlations between individual attributes (Figure 4). Particularly high correlations or anticorrelations indicates how different datasets are affecting each other and which ones can be jointly used in an interpretation. The correlation matrix between the attributes shows, that in general, the correlation is strongest between attributes derived from the same data type (radar, magnetic or gravity), as would be expected. Interestingly enough, some of the attributes do not follow this general observation. E.g. the Tilt-Derivative of the gravity (TDX grv) correlates stronger with radar roughness, than with any other gravity derived attribute. Roughness reflects first of all variations in the topography itself. Such a varying topography will cause a varying gravity and to a minor portion magnetic signal. That is seen, in the correlations of roughness with the spectral attributes in magnetics and with the gravity signal, which might indicate that a smooth bed-ice transition tends to be less dense and has lower susceptibility.

Some of the attributes show almost no correlation with other attributes, such as Tilt-Derivative of the magnetic field (TDX mag), Gaussian Curvature (K_{Gauss}). An absence of correlation is not necessarily a bad observation, as that might indicate that these attributes are sensitive to different source structures.

Another example is the correlation of the Total Magnetic Field anomaly (Mag) and its detrended version (Detrended mag). While the first shows some degree of correlation to the gravity derived attributes, the second does not. That corresponds to the different sensitivity of the gravity and magnetic field to the sources, but might also indicate that we miss some of the gravity signal by using a gridded data set as input and not measurements along the flight lines.

Other attributes as the roughness attributes (ζ bed, η bed) show a correlation with both gravity and magnetic attributes, for example the spectral centroid (Centroid mag) or the shape index (SI grv). Similarly, the power of the 5 to 15 km bin (Bin Power mag) has a correlation with the basal roughness attributes and could indicate that sedimentary basins lack short-wavelength signals as they tend to have smoother surfaces. Similar, correlations between the gravity attributes could support the idea that dense rocks tend to be more erosion-resistant, leading to rougher landscapes.

https://doi.org/10.5194/egusphere-2025-1905
Preprint. Discussion started: 12 May 2025

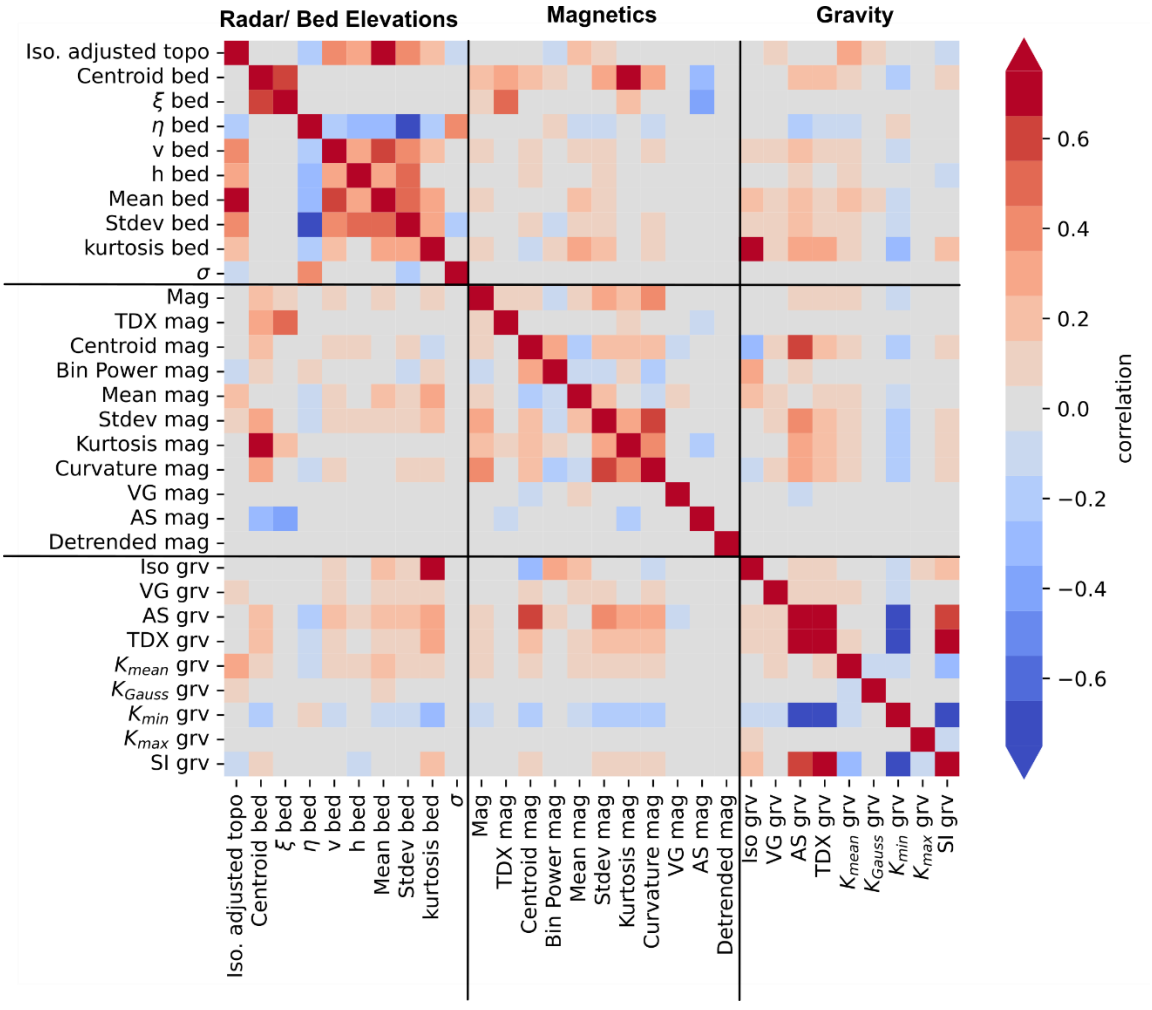

Figure 4: Correlation matrix for all attributes listed in Table 1.

4.2 Weights for individual attributes

335 Before we analyse the SOM in more details with respect to its possible (geological meaning), we show the weights for the individual attributes in Figure 5. As well as the results below, this is not a unique solution, as there are numerous possibilities and parameter sets that potentially yield acceptable results. Additionally, even with the same choice of parameters, the outcome may vary based on the initialisation. Hence, the results presented here, must be seen as an example.

If weights are near zero across the whole map for a specific attribute, that indicates that the attribute has no significant impact
340 on the SOM and could be omitted from the analysis without significant loss of information. The weights map shows that some of the attributes, e.g. SI Grav, strongly influence the results, while others, e.g. Kurtosis mag and bed, have a minor impact. That corresponds to the correlation with other attributes (Figure 4). Those attributes not correlating with other attributes have

https://doi.org/10.5194/egusphere-2025-1905
Preprint. Discussion started: 12 May 2025

in general less impact on the final SOMs, while those showing a larger degree of correlation are deemed more important. That must be taken into consideration when discussing the dependency on the final SOM on the choice of attributes for analysis.

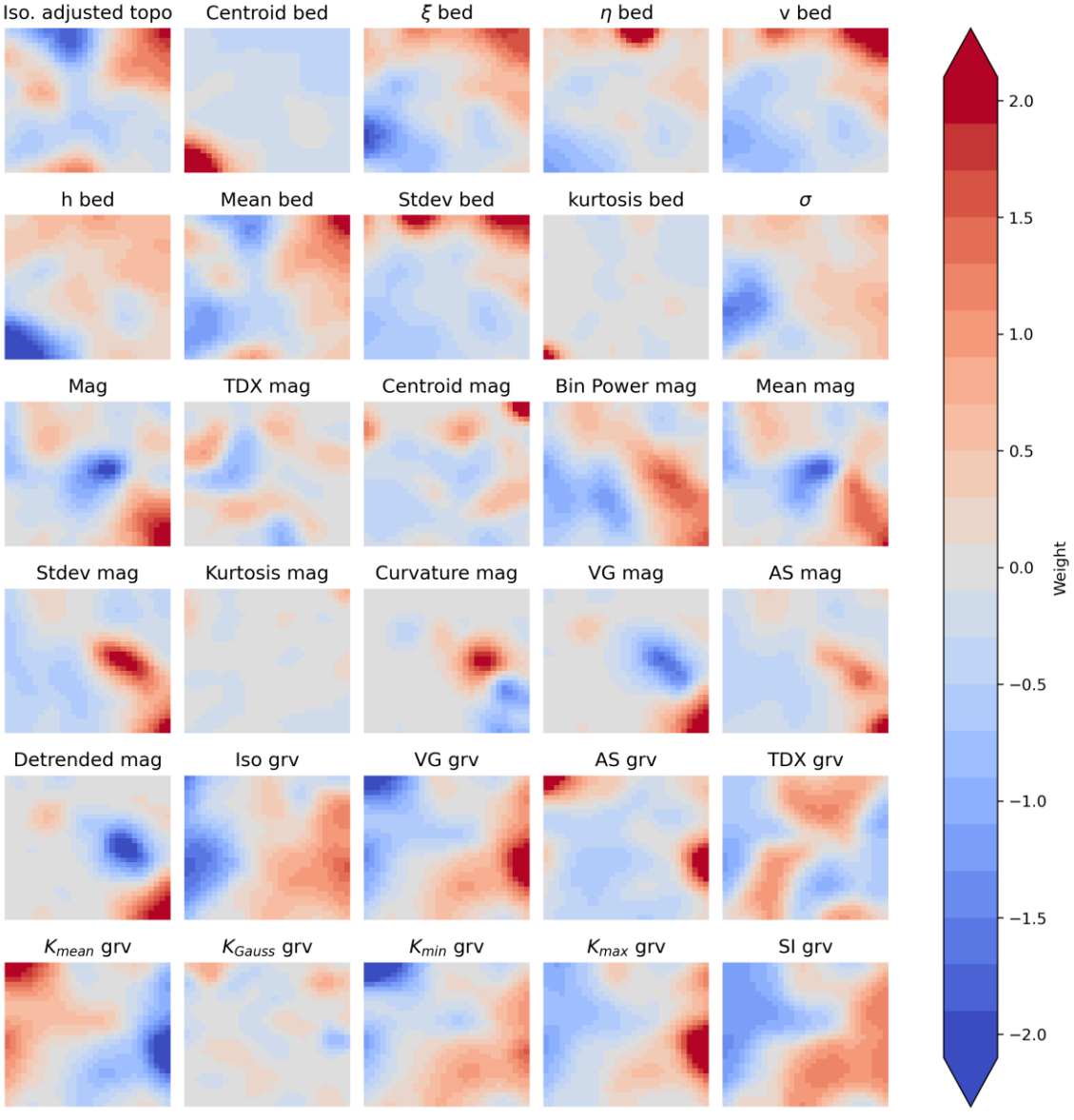

Figure 5 Weights for every attribute and cell of the SOM. All attributes where rescaled using the standard deviation, before the training started.

https://doi.org/10.5194/egusphere-2025-1905
Preprint. Discussion started: 12 May 2025

4.3 Subglacial clusters from SOMs

Now, we analyse the SOMs in more detail by discussing apparent clusters in the map. For a first comparison between our SOM and the bed type classification by Aitken et al. (2023), we map their classification on our 2D representation (Figure 6).

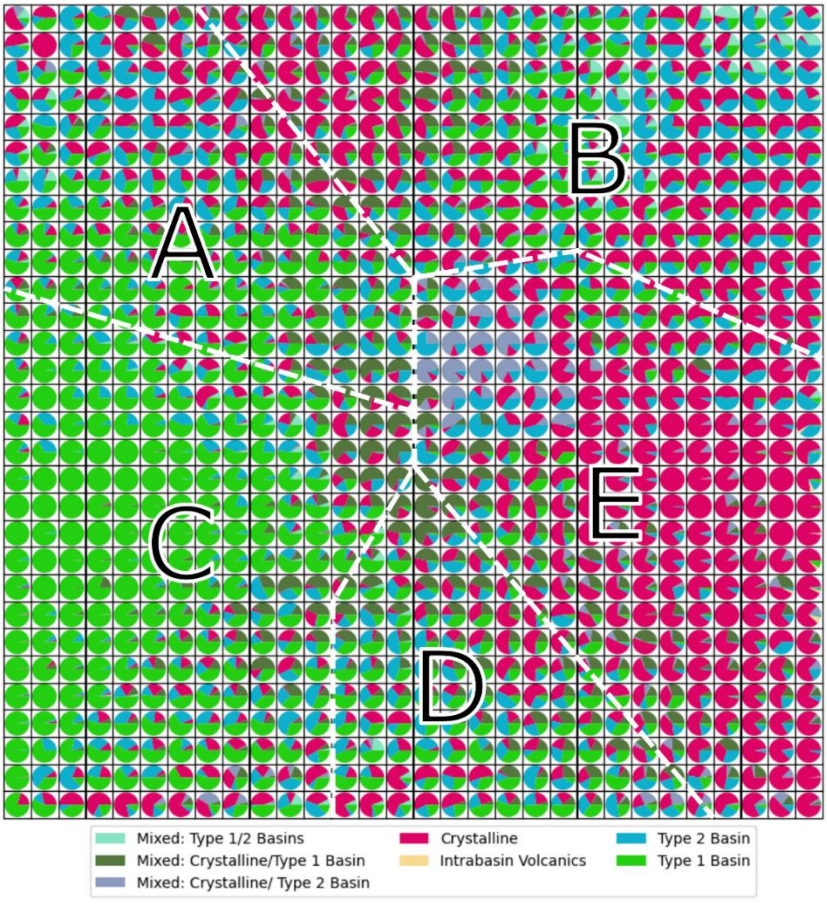

Figure 6 Visualization of the SOM and class distribution. Every data point (measurement on a flight line) was assigned a class according to Aitken et al. (2023) and subsequently mapped onto the SOM. Each cell represents a neuron in the SOM and contains the data points mapped to it. The pie charts within each cell indicate the proportions of different classes present. The letters A–E highlight regions of the SOM with similar properties, they are manually defined to aid description and interpretation.

We shortly summarize the classes from Aitken et al. (2023): The crystalline-basement class indicates where the bed is interpreted to consist of igneous or metamorphic rocks (including high-grade metasedimentary rocks), with either no or only a thin veneer of sedimentary cover. Typically, these regions possess the characteristics of high elevation and high gravity with high spatial variability in topography, gravity, and magnetic data. Type 1 basin class represents regions where sedimentary basins are preserved in relatively unmodified basins, with typical characteristics of low elevation and low gravity, and low

https://doi.org/10.5194/egusphere-2025-1905
Preprint. Discussion started: 12 May 2025

spatial variability in gravity and magnetic data. Along-track roughness tends to be low. The intra-basin volcanics class includes areas where volcanic rocks are interpreted to be emplaced within a Type 1 basin sequence. Type 2 basin class in turn represents areas sedimentary rocks are known or inferred but the original depositional basin is not preserved. These rocks tend to predate the formation of the present landscape, are often uplifted to high elevations, may be intruded by younger igneous rocks, may be heavily eroded and may have geophysical characteristics more similar to crystalline basement than Type 1 basins. Mixed classes are analysis where the geophysical characteristics is not providing clear evidence for an assignment to a single class (see Aitken et al. 2023 for more details on the classification).

We would expect our SOM to be contributing the most to an improved understanding of the mixed or inconclusive classes. Therefore, we sample for each data point of our SOM its class according to Aitken et al. (2023). Figure 6 shows for each cell of our map the percentage of classes present as a pie chart. Form this classification map, we define 5 domains, which have a predominant class. For example, Type 1 basins are predominantly located within cluster C aligning with the expected characteristics of smooth beds, low gravity, and minimal magnetic signals. In contrast, crystalline rocks are predominantly found in the cluster E. This observation supports the assumption that strong magnetic anomalies are typically generated by crystalline rocks. Furthermore, crystalline rocks are also seen in the left side of cluster B. This sub-cluster exhibits high roughness, intense magnetic and gravity signals as expected for crystalline rocks. Type 2 basins, however, do not show a distinct concentration, but are visible across various regions of the map. This dispersion raises questions about the feasibility of coherently inferring this class solely from the attribute compilation used here or from the robustness of defining this class over such a large region. Possibly, the Type 2 basins, in this region mainly sedimentary rocks on highlands, have a more heterogenous build-up or reflect different sub-types compared to the interpretation by Aitken et al. (2023). For the mixed class, no clear domain can be found on the SOM conforming their complex nature.

On the map in Figure 7, we show the SOM representations as a map projection from the individual flight lines, and in Figure 8 along a profile through the study area, in order to provide a spatial representation. Please note that the SOM is mapping data firstly in a 2D Domain based on attribute similarity and irrespective of the geographic location (see inset in Figure 7). Hence, the domains A to E seen in Figure 6 and Figure 7 are only to guide visual comparison.

Comparison with the bed type classification of Aitken et al. (2023) shows a general agreement (Figure 7). Particularly, the delineation of various highlands corresponds closely between the two classifications. However, for some structures, as Knox Highlands (classified as Crystalline) and Highlands A (classified as Type 2 Basin), there are differences in the results. This is coherent with the observation that Type 2 Basin class seems to be mapped for quite dissimilar physical settings.

Additionally, most basins, including the Southern Wilkes Basin, Central Aurora Basin, and Aurora South Basin, exhibit strong consistency with the classification presented by Aitken et al. (2023). Furthermore, the sedimentary basin likelihood map as presented by Li et al. (2022) consistently indicates thick sedimentary layers in areas that were mapped within our C. The most significant disagreement between the SOM and the classification by Aitken et al. (2023) is shown for the Sabrina Basin and Aurora North Basin. In these areas, the fine-scale variations within Clusters A, D, and E of the mapped SOM somehow

https://doi.org/10.5194/egusphere-2025-1905
Preprint. Discussion started: 12 May 2025

395 contradict the homogeneous classification by Aitken et al. (2023), indicating that the SOM might be able to add local variations, best seen when compared along an individual flight line (Figure 8).

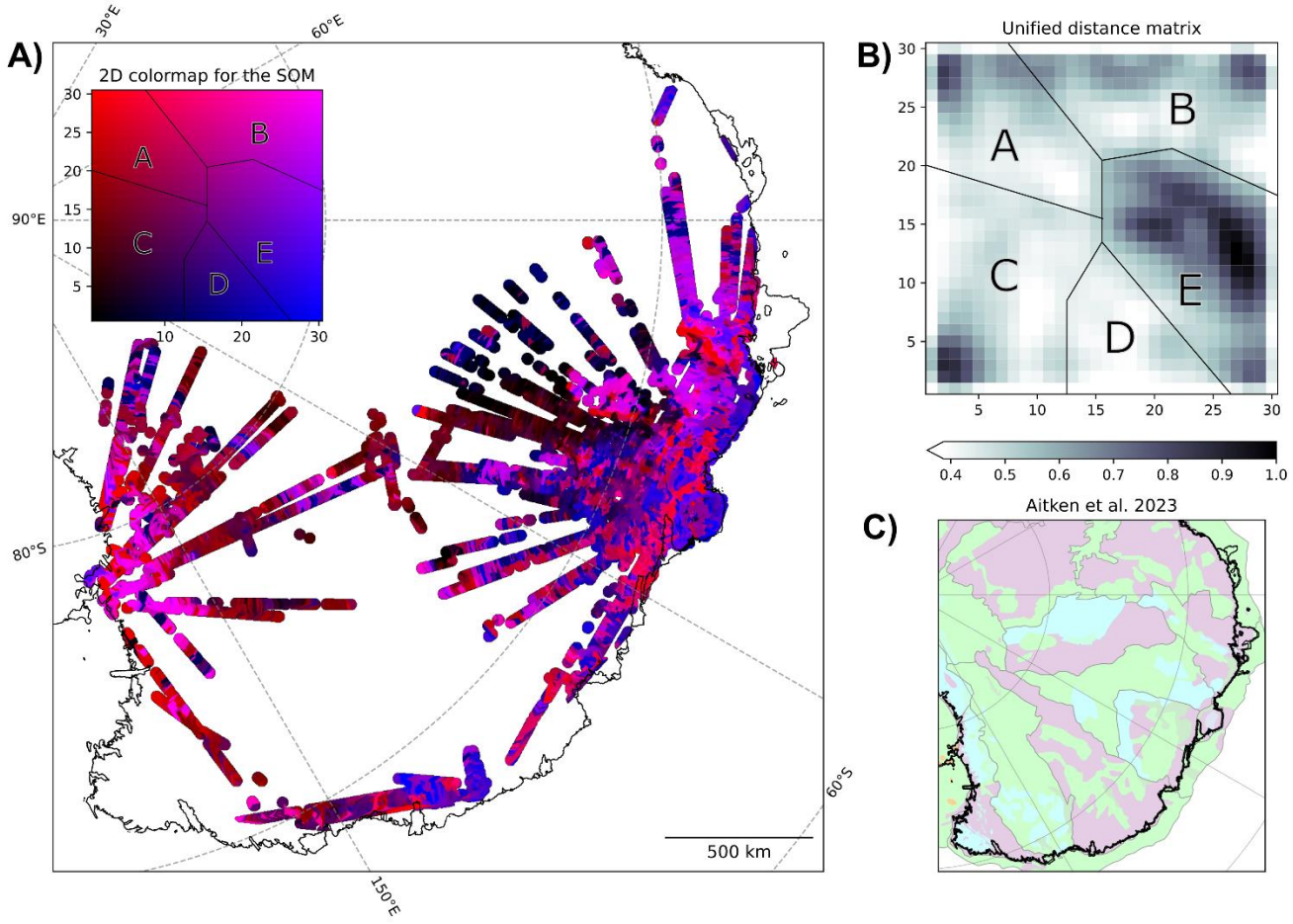

Figure 7: Representation of the clusters from the SOM. A) Geographical distribution of the SOM., B) Unified distance matrix for the presented SOM. C) Classification of geological bed type from Aitken et al. (2023). Yellow line indicates profile of Figure 8.

400 Along a flight line (Figure 8) the interpretation by Aitken et al. (2023) does not clearly follow the boundaries visible in the data and SOM. The radar data show that there are sections of the basin where no return from the bed was detected (e.g. distance ~100 km), while it appears as a very smooth reflector in places where it was detected (~140 km). Additionally, the magnetic signal exhibits a predominantly long wavelength above the basin and shows no obvious correlation with the bed. These observations indicate the presence of non-magnetic rocks near the bed. The SOM effectively captures the abrupt change at the
405 rise of Aurora North Basin in the north of the profile (Figure 8). For the clusters B and E the correlation between the magnetic signal and bed elevation becomes evident. This suggests the presence of magnetic rocks near the surface of Aurora North Basin, whereas it is not the case in the Aurora Basin. This illustrates how the SOM can successfully integrate information from

https://doi.org/10.5194/egusphere-2025-1905
Preprint. Discussion started: 12 May 2025

various data types into a single parameter clearly highlighting the most probable geological boundaries. It therefore could be a useful tool for future mapping attempts and could also help adjusting boundaries while leveraging all available data types.

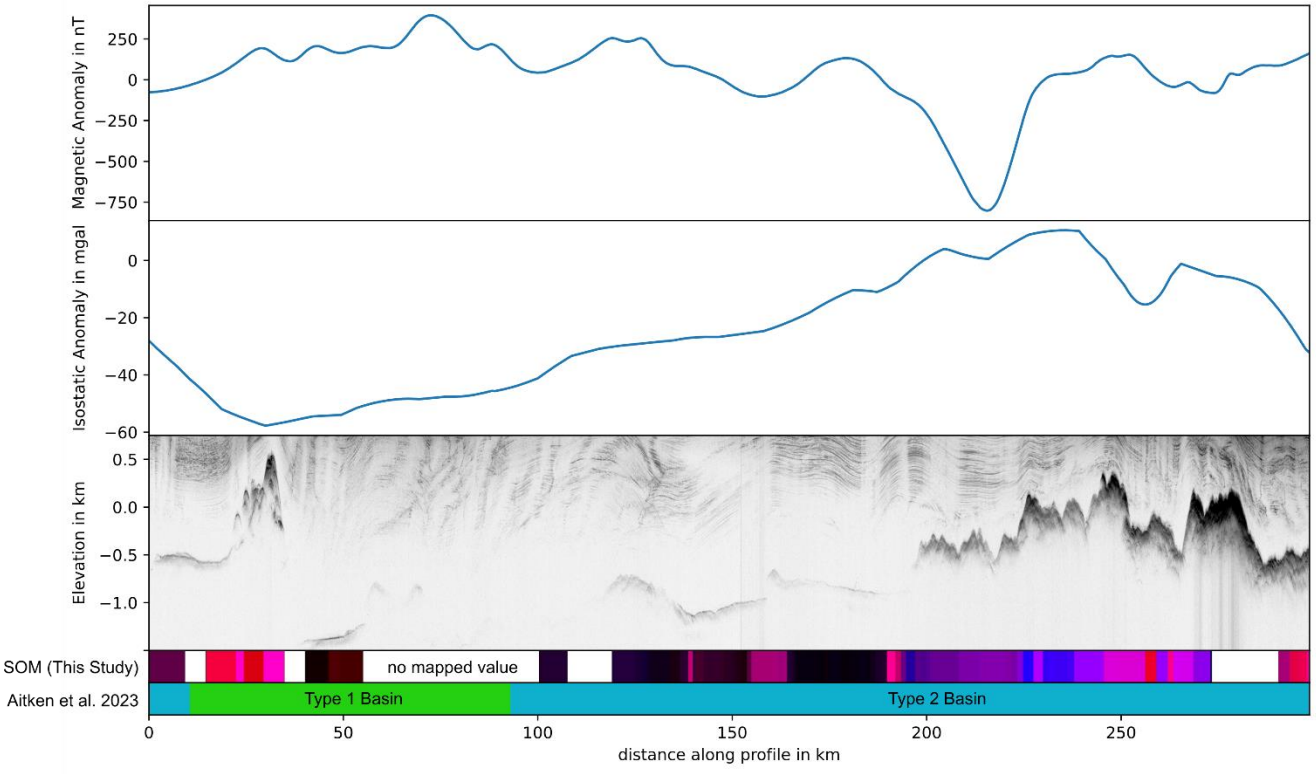

Figure 8: A combined plot of magnetics, gravity and radar data along a profile. Beneath the plots, the SOM is shown and the classification by Aitken et al., 2023. Colour coding for SOMS is according to the inset in Figure 5.

4.4 Pitfalls and possibilities of SOMs

The comparison to the expert judgment approach by Aitken et al. (2023) by compiling available data sources, shows that SOMs can potentially provide an added level of detail or aid in detecting possible errors or inconsistencies as it should be based on measured data as much as possible. Nevertheless, while it seems to be compelling to trust the automatic interpretation of the SOM in comparison to direct studies, one should be aware of the limitations of the method. First of all, the presented choice of attributes is not the only possible choice. While many attributes included in our analysis show high correlation (Fig. 4), it is important not to omit attributes that may show highly similar features. However, a balanced approach is important and focusing too much on a certain kind of attribute or dataset might distort the outcome. Other attributes derived from the presented datasets or even other independent datasets like roughness derived from ice surface elevation or ice flow velocity could be added. Others might be omitted as for example the use of the gravity field and the vertical gradient seems to add little additional information. In general, it would be preferential to use a consistent data set, possibly line data for all observed fields to improve

https://doi.org/10.5194/egusphere-2025-1905
Preprint. Discussion started: 12 May 2025

interpretation at survey scale. Still, a slight trade-off might be thereby that along-line variations may be underestimated if line orientations are not located perpendicular to the main strike direction.

But this trade-off appears to be preferential to the use of gridded data products, where interpolation and the lower resolution of grids compared to line products, affect the quality of the resulting products. Still, the insensitivity to spatial anisotropy of gridded data products might outweigh the gains in data resolution. Furthermore, additional attributes that can be derived from gridded datasets that potentially enhance the resulting SOMs. Additionally, the utilization of migrated radargrams in combination with a correspondingly adjusted bed elevation dataset could potentially reduce the correlations between roughness and ice thickness. This approach has the potential to produce improved results, with an improved overall resolution and quality of the attributes.

One drawback of the SOMs is that there is little control over the meaning of the output clusters, requiring an interpretation to assign meaning to each cluster. One should mention as well that not all features mapped by the SOMs might be a geological signal, but some, especially local features, might reflect data quality (measurement errors or noise). To generate a well-informed classification, multiple data types should be combined and a careful assessment of the data products is required.

Still, a product like SOMs will greatly assist in defining (geological) units with distinct properties and to aid interpreters to make data-optimised classifications and to understand the support for their interpretations from the data selection. Especially, when zooming in on the geology under the ice and the spatial scale that seems to be most important for understanding the coupling of ice-sheets and the underlying solid earth structure (e.g. McCormack et al. 2022), the SOMs can provide a second level of detail. As always, careful evaluation of the final results is still a crucial point in estimating subglacial properties as the SOMs do not provide immediately a new geological map, but a tool for classification and interpretation.

5 Conclusions

We present a novel form of mapping subglacial geology by using Self-Organizing Maps applied to radar, gravity and magnetic data sets, mimicking flight lines from the NASA Operation Ice Bridge (OIB) dataset in East Antarctica. The attributes calculated from the data sets provide a suite of products useful for interpretation, however, challenging for manual interpretation. Hence, the SOM groups the complex features into an easy to understand common framework.

Comparison to the classification of Aitken et al. (2023) shown in general a good agreement for the major classes in regions of low complexity, but indicates as well the nonunique nature of some classes. In such areas the SOMs can help to refine existing interpretations and unveil previously unknown small-scale structures. To further enhance the clustering capabilities of the SOM, an in-depth exploration of hyperparameters could lead to improved results.

Furthermore, the choice of input datasets by assessing the importance of different attributes is worth exploring in more detail. Here, we limited ourselves to choosing similar number of attributes for the three different kind of data in order to prevent a bias towards a single data set without testing how the results would varying the number of attributes, mainly due to computational reasons, but also due to the different characteristics of the input data set (flight lines and resampled gridded products)-.

https://doi.org/10.5194/egusphere-2025-1905
Preprint. Discussion started: 12 May 2025

In general, data selection is a key to avoid a bias by inconsistent data sets and for example, the recently released geophysical data catalogue from the British Antarctic Survey includes multiple surveys with magnetic, gravity, and radar data (Frémand et al., 2022), presenting an opportunity to further explore the possibilities of SOMs for flight line data.

As a next step, the classification of different bed types could also serve as constraint, a priori information for (joint) inversion, that could extend the analysis from a more description of subglacial properties to a physical earth model, needed to describe the full coupling between the Solid Earth and the overlying ice-sheets.

Code Availability: Code will be released upon acceptance of the paper through Zenodo.

Author contribution: JL carried out the formal analysis and prepared all figures. JL and JE wrote the manuscript draft; KM reviewed and edited the manuscript; JE and KM supervised the study as part of the Master thesis by JL.

Competing interests: The authors declare that they have no conflict of interest.

Acknowledgments: JL acknowledges funding received by the Erasmus+ programme of the European Union which made his stay at the Norwegian Polar Institute in Tromsø possible. We thank Alan Aitken for discussions on an earlier version of this manuscript, which helped us to improve our interpretation.

https://doi.org/10.5194/egusphere-2025-1905
Preprint. Discussion started: 12 May 2025

References

Aitken, A. R. A., Young, D. A., Ferraccioli, F., Betts, P. G., Greenbaum, J. S., Richter, T. G., ... & Siegert, M. J..: The subglacial geology of Wilkes Land, East Antarctica. *Geophysical Research Letters*, *41*(7), 2390-2400, https://doi.org/10.1002/2014GL059405, 2014.

Aitken, A. R. A., Roberts, J. L., Ommen, T. V., Young, D. A., Golledge, N. R., Greenbaum, J. S., ... & Siegert, M. J.:Repeated large-scale retreat and advance of Totten Glacier indicated by inland bed erosion. Nature, 533(7603), 385-389, https://doi.org/10.1038/nature17447, 2016

Aitken, A. R., Li, L., Kulessa, B., Schroeder, D., Jordan, T. A., Whittaker, J. M., ... & Siegert, M. J.: Antarctic sedimentary basins and their influence on ice-sheet dynamics. Reviews of Geophysics, 61(3), e2021RG000767. https://doi.org/10.1029/2021RG000767, 2023.

Anandakrishnan, S., Blankenship, D. D., Alley, R. B., & Stoffa, P. L.: Influence of subglacial geology on the position of a West Antarctic ice stream from seismic observations. *Nature*, *394*(6688), 62-65, https://doi.org/10.1038/27889, 1998.

Bayer, B., Geissler, W. H., Eckstaller, A., & Jokat, W.: Seismic imaging of the crust beneath Dronning Maud Land, East Antarctica. *Geophysical Journal International*, *178*(2), 860-876, https://doi.org/10.1111/j.1365-246X.2009.04196.x, 2009.

Bell, R. E.,: The role of subglacial water in ice-sheet mass balance. *Nature Geoscience*, *1*(5), 297-304, https://doi.org/10.1038/ngeo186 , 2008.

Betts, P. G., Moore, D., Aitken, A., Blaikie, T., Jessell, M., Ailleres, L., ... & Chukwu, C.: Geology from aeromagnetic data. *Earth-Science Reviews*, 104958, https://doi.org/10.1016/j.earscirev.2024.104958, 2024.

Blakely, R. J.: *Potential theory in gravity and magnetic applications*. Cambridge University Press, https://doi.org/10.1017/CBO9780511549816, 1996.

Blankenship et al.,: IceBridge HiCARS 2 L2 Geolocated Ice Thickness, Version 1. DOI:10.5067/9EBR2T0VXUDG. https://nsidc.org/data/IR2HI2/versions/1, 2012.

Blankenship et al.: IceBridge HiCARS 1 L1B Time-Tagged Echo Strength Profiles, Version 1. DOI: 10.5067/W2KXX0MYNJ9G. https://nsidc.org/data/IR1HI1B/versions/1, 2017.

Colgan, W., Wansing, A., Mankoff, K., Lösing, M., …, Ebbing, J., et al.: Greenland Geothermal Heat Flow Database and Map (Version 1), Earth Syst. Sci. Data, 14(5), 2209-2238, https://doi.org/10.5194/essd-14-2209-2022, 2022.

Davison, B. J., Hogg, A. E., Gourmelen, N., Jakob, L., Wuite, J., Nagler, T., ... & Engdahl, M. E.: Annual mass budget of Antarctic ice shelves from 1997 to 2021. *Science Advances*, *9*(41), eadi0186. https://doi.org/10.1126/sciadv.adi0186, 2023.

Ebbing, J., Haas, P., Ferraccioli, F., Pappa, F., Szwillus, W., & Bouman, J.: Earth tectonics as seen by GOCE- Enhanced satellite gravity gradient imaging. *Scientific reports*, *8*(1), 16356, https://doi.org/10.1038/s41598-018-34733-9, 2018.

Eisen, O., Winter, A., Steinhage, D., Kleiner, T., & Humbert, A.: Basal roughness of the East Antarctic Ice Sheet in relation to flow speed and basal thermal state. *Annals of Glaciology*, *61*(81), 162-175, https://doi.org/10.1017/aog.2020.47, 2020.

Elliot, D. H.: Tectonics of Antarctica: a review. Am. J. Sci, 275, 45-106, 1975.

https://doi.org/10.5194/egusphere-2025-1905
Preprint. Discussion started: 12 May 2025

Ferraccioli, F., Bozzo, E., & Damaske, D.: Aeromagnetic signatures over western Marie Byrd Land provide insight into magmatic arc basement, mafic magmatism and structure of the Eastern Ross Sea Rift flank. *Tectonophysics*, *347*(1-3), 139-165, https://doi.org/10.1016/S0040-1951(01)00242-6, 2002.

Ferraccioli, F., Armadillo, E., Jordan, T., Bozzo, E., & Corr, H.: Aeromagnetic exploration over the East Antarctic Ice Sheet: a new view of the Wilkes Subglacial Basin. *Tectonophysics*, *478*(1-2), 62-77, https://doi.org/10.1016/j.tecto.2009.03.013, 2009.

Fretwell, P., Pritchard, H. D., Vaughan, D. G., Bamber, J. L., Barrand, N. E., Bell, R., ... & Zirizzotti, A.: Bedmap2: improved ice bed, surface and thickness datasets for Antarctica. The cryosphere, 7(1), 375-393, https://doi.org/10.5194/tc-7-375-2013, 2013.

Golynsky, A., Chiappini, M., Damaske, D., Ferraccioli, F., Finn, C. A., Ishihara, T., ... & von Frese, R.: ADMAP—A digital magnetic anomaly map of the Antarctic. *Antarctica: Contributions to global earth sciences*, 109-116, https://doi.org/10.1007/3-540-32934-X_12, 2006.

Golynsky, A. V., Ferraccioli, F., Hong, J. K., Golynsky, D. A., Von Frese, R. R. B., Young, D. A., ... & Roberts, J. L.: New magnetic anomaly map of the Antarctic. Geophysical Research Letters, 45(13), 6437-6449, https://doi.org/10.1029/2018GL078153, 2018.

Jamieson, S. S., Stokes, C. R., Ross, N., Rippin, D. M., Bingham, R. G., Wilson, D. S., ... & Bentley, M. J.: The glacial geomorphology of the Antarctic ice sheet bed. *Antarctic Science*, *26*(6), 724-741, https://doi.org/10.1017/S0954102014000212, 2014.

Jordan, T. A., Ferraccioli, F., Corr, H., Graham, A., Armadillo, E., & Bozzo, E.: Hypothesis for mega-outburst flooding from a palaeo-subglacial lake beneath the East Antarctic Ice Sheet. *Terra Nova*, *22*(4), 283-289, https://doi.org/10.1111/j.1365-3121.2010.00944.x, 2010.

Jordan, T. A., Riley, T. R., & Siddoway, C. S.: The geological history and evolution of West Antarctica. Nature Reviews Earth & Environment, 1(2), 117-133, https://doi.org/10.1038/s43017-019-0013-6, 2020.

Jordan, T. A., Thompson, S., Kulessa, B., & Ferraccioli, F.: Geological sketch map and implications for ice flow of Thwaites Glacier, West Antarctica, from integrated aerogeophysical observations. *Science Advances*, *9*(22), eadf2639, hhttps://doi.org/10.1126/sciadv.adf26, 2023.

Kim, H. R., Golynsky, A. V., Golynsky, D. A., Yu, H., Von Frese, R. R. B., & Hong, J. K.: New magnetic anomaly constraints on the Antarctic crust. *Journal of Geophysical Research: Solid Earth*, *127*(3), e2021JB023329, https://doi.org/10.1029/2021JB023329, 2022.

Klose, C. D.: Self-organizing maps for geoscientific data analysis: geological interpretation of multidimensional geophysical data. *Computational Geosciences*, *10*, 265-277, https://doi.org/10.1007/s10596-006-9022-x, 2006.

Koellner, S., Parizek, B. R., Alley, R. B., Muto, A., & Holschuh, N.: The impact of spatially-variable basal properties on outlet glacier flow. *Earth and Planetary Science Letters*, *515*, 200-208, https://doi.org/10.1016/j.epsl.2019.03.026, 2019.

Kohonen, T.: The self-organizing map. Proceedings of the IEEE, 78(9), 1464-1480, https://doi.org/ 10.1109/5.58325, 1990.

https://doi.org/10.5194/egusphere-2025-1905
Preprint. Discussion started: 12 May 2025

Leitchenkov, G. L., Antonov, A. V., Luneov, P. I., & Lipenkov, V. Y.: Geology and environments of subglacial Lake Vostok. *Philosophical Transactions of the Royal Society A: Mathematical, Physical and Engineering Sciences*, *374*(2059), 20140302, https://doi.org/10.1098/rsta.2014.0302, 2016.

Li, X.: Curvature of a geometric surface and curvature of gravity and magnetic anomalies. *Geophysics*, *80*(1), G15-G26, https://doi.org/10.1190/geo2014-0108.1. 2015.

Li, L., Aitken, A. R., Lindsay, M. D., & Kulessa, B.: Sedimentary basins reduce stability of Antarctic ice streams through groundwater feedbacks. Nature Geoscience, 15(8), 645–650. https://doi.org/10.1038/s41561-022-00992-5, 2022.

Li, L., Xiao, E., Wei, X., Qiu, N., Latif, K., Guo, J., & Sun, B.: Crustal Imaging across the Princess Elizabeth Land, East Antarctica from 2D Gravity and Magnetic Inversions. *Remote Sensing*, *15*(23), 5523, https://doi.org/10.3390/rs15235523, 2023.

Liebsch, J.: Combined analysis of airborne geophysical data using machine learning to obtain sub-ice geology in East Antarctica. Master thesis at Kiel University, unpublished, 2023.

Lösing, M., & Ebbing, J.: Predicting geothermal heat flow in Antarctica with a machine learning approach. Journal of Geophysical Research: Solid Earth, 126(6), e2020JB021499, https://doi.org/10.1029/2020JB021499, 2021.

Lowe, M., Jordan, T., Ebbing, J., Koglin, N., Ruppel, A., Moorkamp, M., ... & Larter, R.: Comparing geophysical inversion and petrophysical measurements for northern Victoria Land, Antarctica. *Geophysical Journal International*, *239*(1), 276-291, ttps://doi.org/10.1093/gji/ggae272, 2024a.

Lowe, M., Jordan, T., Moorkamp, M., Ebbing, J., Green, C., Lösing, M., ... & Larter, R.: The 3D crustal structure of the Wilkes Subglacial Basin, East Antarctica, using variation of information joint inversion of gravity and magnetic data. *Journal of Geophysical Research: Solid Earth*, *129*(10), e2023JB027794, https://doi.org/10.1029/2023JB027794 2024b.

Matsuoka, K.: Pitfalls in radar diagnosis of ice-sheet bed conditions: Lessons from englacial attenuation models. *Geophysical Research Letters*, *38*(5). https://doi.org/10.1029/2010GL046205, 2011.

MacGregor, J. A., Boisvert, L. N., Medley, B., Petty, A. A., Harbeck, J. P., Bell, R. E., ... & Yungel, J. K.: The scientific legacy of NASA's Operation IceBridge. Reviews of Geophysics, 59, e2020RG000712. https://doi.org/10.1029/2020RG000712, 2021.

McCormack, F. S., Roberts, J. L., Dow, C. F., Stål, T., Halpin, J. A., Reading, A. M., & Siegert, M. J.: Fine-scale geothermal heat flow in Antarctica can increase simulated subglacial melt estimates. *Geophysical Research Letters*, *49*(15), e2022GL098539, https://doi.org/10.1029/2022GL098539, 2022.

McLean, M. A., Wilson, C. J. L., Boger, S. D., Betts, P. G., Rawling, T. J., & Damaske, D.: Basement interpretations from airborne magnetic and gravity data over the Lambert Rift region of East Antarctica. *Journal of Geophysical Research: Solid Earth*, *114*(B6), https://doi.org/10.1029/2008JB005650, 2009.

Morlighem, M., Rignot, E., Binder, T., Blankenship, D., Drews, R., Eagles, G., ... & Young, D. A.: Deep glacial troughs and stabilizing ridges unveiled beneath the margins of the Antarctic ice sheet. Nature geoscience, 13(2), 132-137. https://doi.org/10.1038/s41561-019-0510-8, 2020.

https://doi.org/10.5194/egusphere-2025-1905
Preprint. Discussion started: 12 May 2025

Morlighem, M.: MEaSUREs BedMachine Antarctica, Version 3. [BED ELEVATION]. Boulder, Colorado USA. NASA National Snow and Ice Data Center Distributed Active Archive Center. https://doi.org/10.5067/FPSU0V1MWUB6, 2022. [last accessed 25/02/2025]

Mouginot, J., Scheuchl, B. and E. Rignot, E.,: MEaSUREs Annual Antarctic Ice Velocity Maps 2005-2017, Version 1. Boulder, Colorado USA. NASA National Snow and Ice Data Center Distributed Active Archive Center https://doi.org/10.5067/9T4EPQXTJYW9, 2017 [last accessed 25/02/2025]

Nagy, D., Papp, G., & Benedek, J.: The gravitational potential and its derivatives for the prism. *Journal of Geodesy*, *74*, 552-560, https://doi.org/10.1007/s001900000116, 2000.

Rignot, E., Jacobs, S., Mouginot, J., and B. Scheuchl, B.: Ice shelf melting around Antarctica, *Science*, 341(6143), 266–270, https://doi.org/10.1126/science.1235798, 2013.

Rippin, D. M., Bingham, R. G., Jordan, T. A., Wright, A. P., Ross, N., Corr, H. F., ... & Siegert, M. J.: Basal roughness of the Institute and Möller Ice Streams, West Antarctica: Process determination and landscape interpretation. *Geomorphology*, *214*, 139-147, https://doi.org/10.1016/j.geomorph.2014.01.021, 2014.

Salem, A., Williams, S., Fairhead, D., Smith, R., & Ravat, D.: Interpretation of magnetic data using tilt-angle derivatives. *Geophysics*, *73*(1), L1-L10, https://doi.org/10.1190/1.2799992, 2008.

Scheinert, M., Ferraccioli, F., Schwabe, J., Bell, R., Studinger, M., Damaske, D., ... & Richter, T. D. (2016). New Antarctic gravity anomaly grid for enhanced geodetic and geophysical studies in Antarctica. *Geophysical Research Letters*, *43*(2), 600-610, https://doi.org/10.1002/2015GL067439, 2016.

Shepherd, T., Bamber, J. L., & Ferraccioli, F.: Subglacial geology in Coats Land, East Antarctica, revealed by airborne magnetics and radar sounding. *Earth and Planetary Science Letters*, *244*(1-2), 323-335, https://doi.org/10.1016/j.epsl.2006.01.068, 2006.

Stål, T., Reading, A. M., Halpin, J. A., & Whittaker, J. M.: Antarctic geothermal heat flow model: Aq1. *Geochemistry, Geophysics, Geosystems*, *22*(2), e2020GC009428, https://doi.org/10.1029/2020GC009428, 2021.

Taylor, G. (1914). Physiography and glacial geology of East Antarctica. The Geographical Journal, 44(4), 365-382, 1914.

Vettigli, G.: MiniSom: minimalistic and NumPy-based implementation of the Self Organizing Map. URL: https://github.com/JustGlowing/minisom/, 2018.

Whitehouse, P. L., Gomez, N., King, M. A., & Wiens, D. A.: Solid Earth change and the evolution of the Antarctic Ice Sheet. *Nature communications*, *10*(1), 503, https://doi.org/10.1038/s41467-018-08068-y, 2019.

Wu, G., Ferraccioli, F., Zhou, W., Yuan, Y., Gao, J., & Tian, G.: Tectonic Implications for the Gamburtsev Subglacial Mountains, East Antarctica, from Airborne Gravity and Magnetic Data. *Remote Sensing*, *15*(2), 306, https://doi.org/10.3390/rs15020306, 2023.

Young, D. A., Wright, A. P., Roberts, J. L., Warner, R. C., Young, N. W., Greenbaum, J. S., ... & Siegert, M. J.: A dynamic early East Antarctic Ice Sheet suggested by ice-covered fjord landscapes. Nature, 474(7349), 72-75, https://doi.org/10.1038/nature10114, 2011.

https://doi.org/10.5194/egusphere-2025-1905
Preprint. Discussion started: 12 May 2025

Zoet, L. K., & Iverson, N. R.: A slip law for glaciers on deformable beds. *Science*, *368*(6486), 76-78, https://doi.org/10.1126/science.aaz1183, 2020.